Ferritic Ductile Cast Iron Damaging Characterization

V. Di Cocco and F. Iacoviello

Università di Cassino, Di.M.S.A.T., via G. Di Biasio 43, 03043 Cassino (FR), Italy, iacoviello@unicas.it

ABSTRACT. *Ductile cast irons are widely used due to their interesting mechanical properties combination (high ductility, high tensile strength, good wear resistance). Graphite nodules peculiarities (roundness, referred to as nodularity, but also graphite elements number per area unit and volume fraction) and matrix microstructure (both chemical composition and heat treatment controlled) strongly affect mechanical behaviour and damaging micromechanisms, also considering very simple loading conditions (e.g. tensile test conditions). Focusing ferritic ductile irons, matrix – graphite nodule debonding, and the consequent voids growth, is often identified as the main damaging micromechanism, and numerous studies provided analytical laws to describe growth of a single void, depending on the void geometries and matrix behaviour. In this work, ferritic DCI damaging micromechanisms were investigated, considering uniaxial tensile tests, and investigating the influence of triaxiality and strain rate. Step by step tensile tests were performed on unnotched and notched specimens. Specimens surfaces were observed by means of a scanning electron microscope (SEM) during the test. Furthermore, tensile test were performed considering different deformation rates, performing a SEM observation of fracture surfaces. Experimental results analysis confirm that matrix-graphite nodules debonding is only one of the damaging micromechanisms involved in ferritic ductile irons failure.*

INTRODUCTION

Ductile cast irons (DCIs) are characterized by high strength and toughness and in the last decades are commercially available as enginnering materials for many applications (e.g. wheels, gears, crankshafts in cars and trucks etc.), replacing both malleable cast irons and forging and cast steels. Matrix plays a key role determining the overall properties combination and allowing to obtain high ductility values (up to more than 18%) and high strength (up to 850 MPa and, considering austempered DCIs, up to 1600 MPa), with a good wear resistance. Matrix names are usually used to designate spheroidal cast iron types [1, 2], Fig. 1:

- ferritic DCIs are characterized by good ductility, with tensile strength values that are equivalent to a low carbon steel.
- pearlitic DCIs show high strength values, good wear resistance and moderate ductility.
- ferritic-pearlitic grades properties are intermediate between ferritic and pearlitic ones.

- martensitic DCIs show very high strength, but low levels of toughness and ductility.
- bainitic grades are characterized by high hardness.
- austenitic DCIs show good corrosion resistance, good strength and dimensional stability at high temperature.
- austempered grades show a very high wear resistance and fatigue strength.

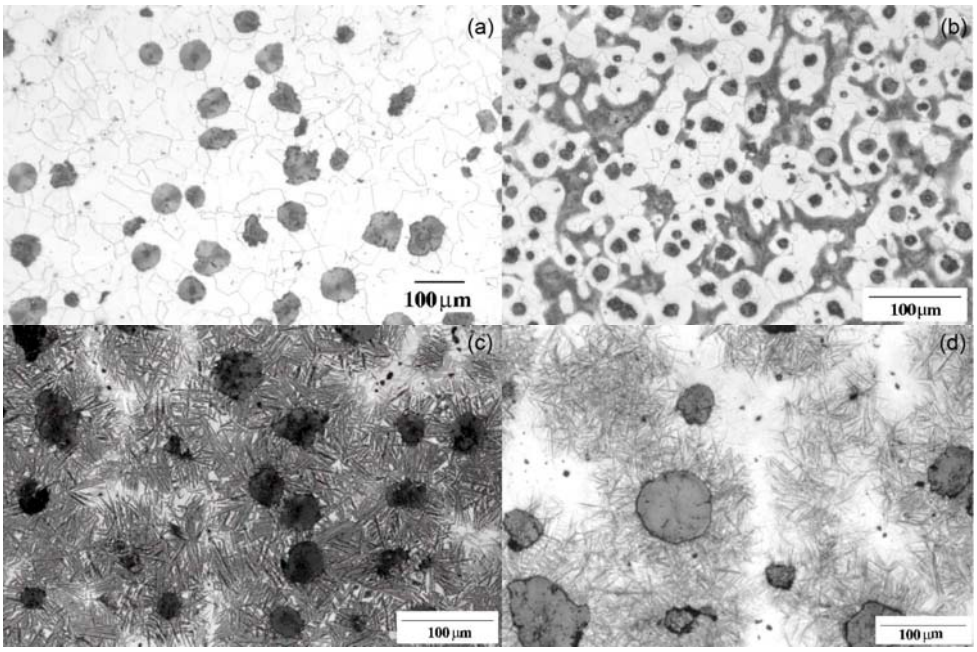

Figure 1: Different DCIs microstructures [3]: a) ferritic, b) ferritic - pearlitic, c) austempered (350°C - 64 min), d) austempered (250° - 50 min).

DCIs damage micromechanisms analysis is usually mainly focused on voids nucleation and growth due to the matrix-graphite nodules debonding [4-8] and numerous studies provided analytical laws to describe a single void growth, depending on the void geometries and matrix behaviour. DCI damage evolution is commonly summarized considering the following steps:
- Separating between nodular graphite and matrix under low stress.
- Plastic deformation in matrix around nodular graphite.
- Initiation of microcracks in deformed matrix between nodular graphite.
- Linkage of graphites by microcracks and formation of larger microcracks.
- Linkage of main crack and selected microcracks to form macrocracks.

Focusing the behaviour of a ductile iron with a completely ferritic matrix [4], no damage at graphite nodule interface was observed in the ‘‘elastic’’ part of the load-displacement curve. Few slip lines were observed emanating from the equator of the nodules, indicating a local plastic deformation of the matrix. Decohesions appeared at the pole cap of the nodules when the macroscopic yield stress was reached (Fig. 2a). Increasing macroscopic plastic deformation induced void growth in the stress direction,

thus forming ellipsoidal cavities inside which nearly undeformed nodules were embedded (Fig. 2b), failure occurred by shear instabilities linking adjacent voids.

Different matrix microstructure could imply a different role played by graphite nodules. Completely pearlitic DCI [9] is characterized by the absence of irreversible damage only for very low stress values (Fig. 3a). An irreversible damage is observed already in the elastic stage (Fig. 3b): cracks could initiate and develop at the graphite nodules pole cap but also cracks initiation and propagation in pearlitic matrix is observed. Stress increase implies both cracks propagation in graphite nodules, and matrix plastic deformation and cracks propagation in pearlitic matrix. Matrix–graphite elements debonding is only rarely observed and cracks propagate inside graphite nodules.

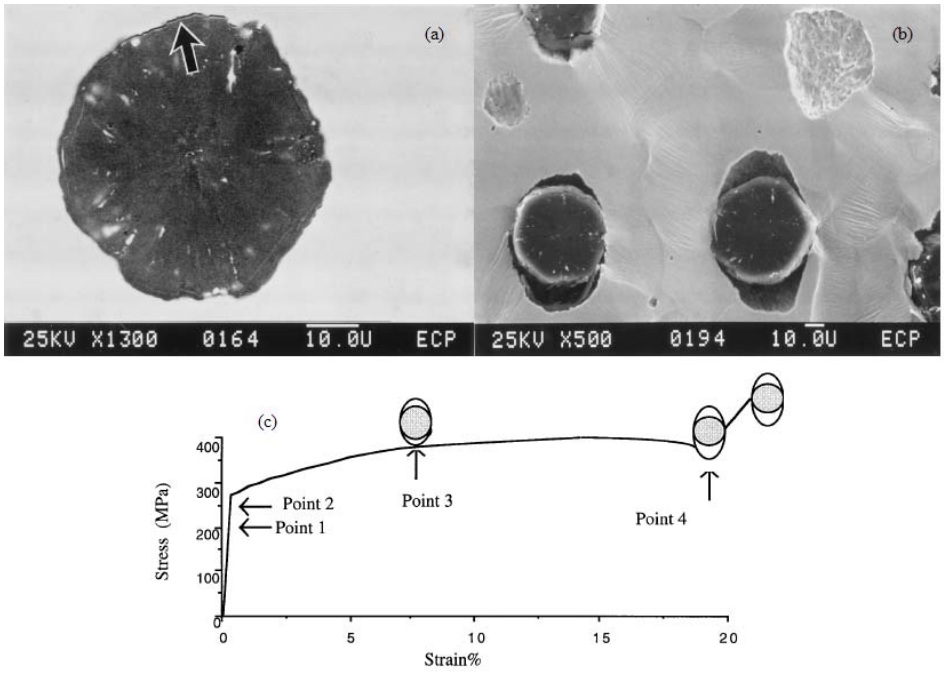

Figure 2: Matrix-graphite nodules debonding evolution during tensile test [4].
a) decohesion of the interface observed in the SEM at point 2 of the stress-strain curve;
b) cavity growth around nodules (point 3 of the stress-strain curve SEM observation);
c) Stress-strain curve recorded during a tensile test.

Considering austempered DCIs [10], fracture could initiate both at graphite nodules – matrix interfaces initiation and in graphite nodules (Fig. 4a); further deformation implies that microcracks inside graphite nodule propagation and connection, with a conseguent complete graphite nodule (Fig. 4b). According to Dai et alii [10], graphite nodules in austempered DCIs cannot be regarded as a voids with no strength and they do not cause micro-notch stress concentration by itself.

The aim of this work was the analysis of damaging micromechanisms in a ferritic DCI. Step by step tensile tests were performed considering quasi – standard and

notched specimens: their surfaces were observed by means of a scanning electron microscope (SEM) during the tensile test. Furthermore, tensile test were performed considering different deformation rates.

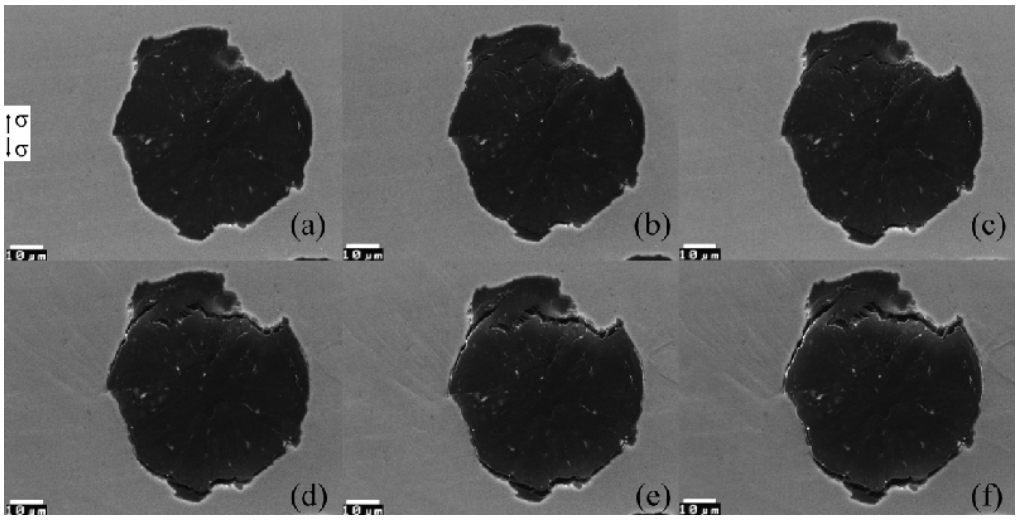

Figure 3. EN GJS700-2 ductile cast iron (100% pearlite). SEM in situ surface analysis corresponding to the following σ [MPa]–ε% values: (a) 130–1%, (b) 520–3.5%, (c) 600–4%, (d) 760–6%, (e) 810–8.5% and (f) 840–10.5% [9].

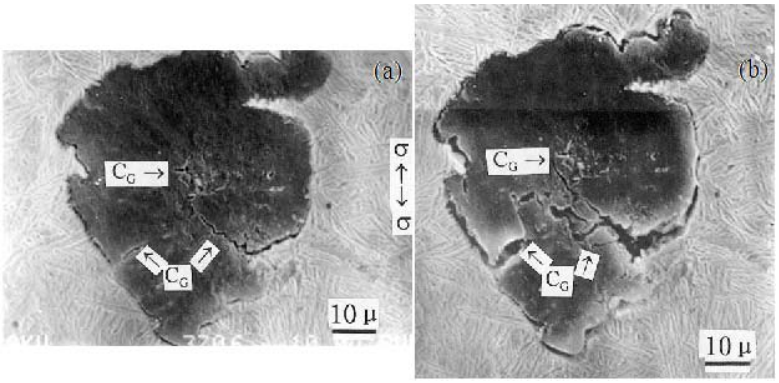

Figure 4. Cracking of a graphite nodule [10]. (a) Microcrack inside a graphite nodule (C_G) at Δl=70 μm; (b) graphite nodule completely cracked at Δl=110 μm.

MATERIAL AND EXPERIMENTAL PROCEDURE

A fully ferritic EN GJS350-22 DCI was considered (Table 1). Graphite elements were characterized by a very high nodularity, higher than 85%, with a volume fractions of about 9-10%. Investigated DCI was cut into microtensile specimens with a length x width x thickness equal to 25 x 2 x 1 mm, respectively. Specimens were ground and

polished and pulled intermittently with a tensile holder and observed in situ using a SEM, considering at least 20 graphite elements (strain rate equal to $9.2 x10^{-5}$ s^{-1}). During tensile tests, specimen deformation and applied load were measured by means of a Linear Variable Differential Transformer (LVDT) and two miniature load cell (10 kN each), respectively. Figures 5a and 5b show the tensile holder with the microtensile specimen and the tensile test machine, respectively.

In order to perform a deeper investigation of damaging micromechanisms, the influence of two parameter was investigated: triaxiality and strain rate.

Triaxiality influence analysis on damaging micromechanism was performed considering notched microspecimens (Fig. 6): SEM analysis was perfomed “in situ”, focusing nodules in the notch zone.

Strain rate influence was investigated by means of tensile tests performed according to standard procedure. Two different strain rates were considered ($1.3x10^{-6}$ s^{-1} and $6.7x10^{-2}$ s^{-1}) and fracture surfaces were investigated by means of a SEM.

Table 1. Ductile cast iron EN GJS350-22 chemical composition (100% ferrite).

C	Si	Mn	S	P	Cu	Cr	Mg	Sn
3.66	2.72	0.18	0.013	0.021	0.022	0.028	0.043	0.010

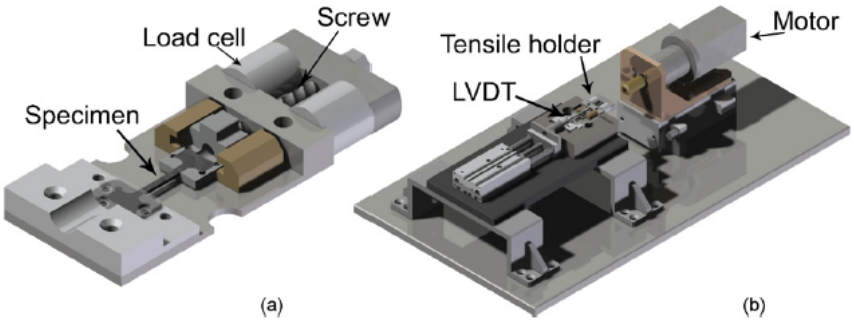

Figure 5. Tensile holder with microtensile specimen (a) and tensile test machine (b).

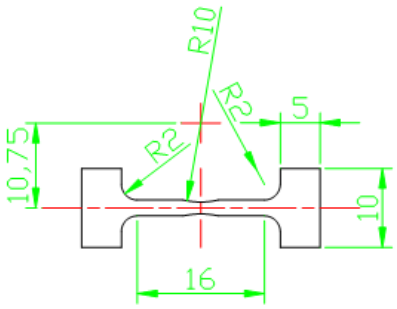

Figure 6. Notched microtensile specimens (1 mm thick).

EXPERIMENTAL RESULTS

Experimental results showed that damaging micromechanism are stress level dependent. Considering tensile test results obtained on unnotched tensile microspecimens, elastic deformation stage is characterized by the absence of cracks or microvoids initiations both in matrix and in graphite elements (Fig. 7a and b, and 8a and b).

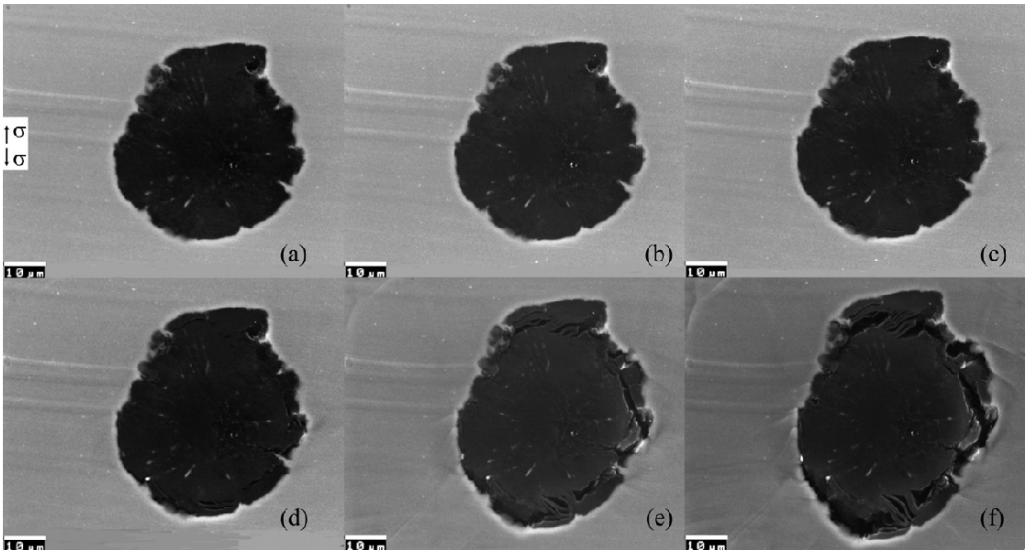

Figure 7. EN GJS350-22 ductile cast iron. SEM in situ surface analysis corresponding to the following σ [MPa]–ε% values: (a) 200–1%, (b) 400–2.5%,(c) 430–5%, (d) 470–7.5%, (e) 490–12.5% and (f) 500–17.5%.

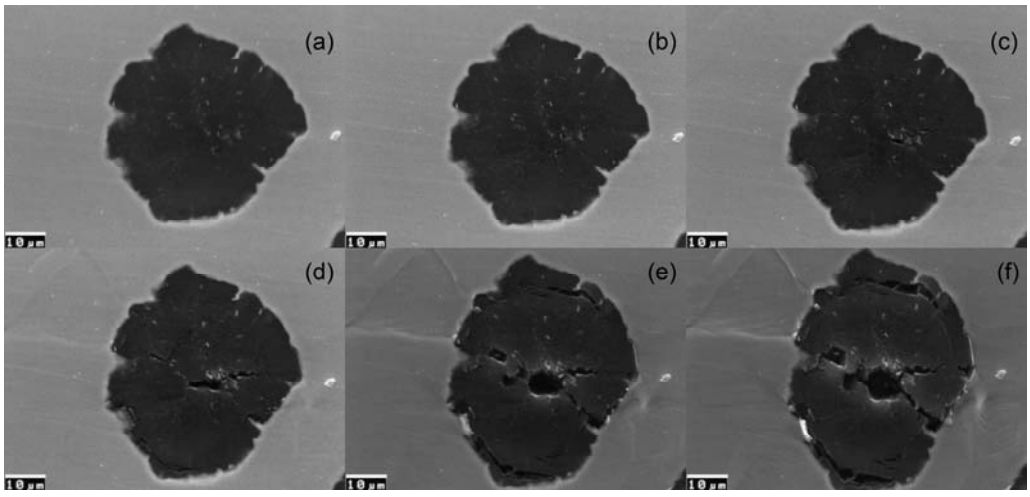

Figure 8. EN GJS350-22 ductile cast iron. SEM in situ surface analysis corresponding to σ [MPa]–ε% values as reported in Fig. 7.

Corresponding to plastic deformation stage, cracks could initiate and develop in graphite elements with an “onion-like” morphology (Fig. 7c and d) and, only corresponding to very high strain values, matrix plastic deformation becomes evident: few slip lines emanate from the equator of the nodules, thus indicating a local plastic deformation of the matrix (Fig. 7e and f). Another damaging mechanism consists in a crack initiation in the center of graphite spheroid (Fig. 8c): crack inside graphite nodule propagates with the increase of the stress value (Fig. 8d). In this case, “onion-like” mechanism is obtained only corresponding to higher stress values (Fig. 8e and f). However, no “pure” ferritic matrix–graphite elements debonding is observed.

Evidences of ferritic matrix plastic deformation (slip lines) are obtained only after cracks initiation in graphite nodules. Considering Fig. 9, and focusing the graphite nodule on the right, it is evident that the very first damage consists in crack initiation in the center of grafite spheroid (Fig. 9a). The increase of the stress value implies a crack propagation in graphite element and the emanation of slip lines (Fig. 9b). Further increase of the stress value implies a propagation of an irreversible damaging of the graphite spheroid on the left (Fig. 9c), with crack that initiate from the interface graphite-matrix, corresponding to the slip lines.

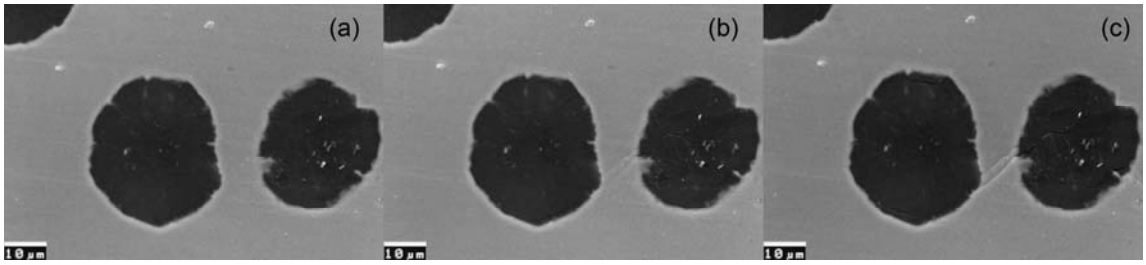

Figure 9. EN GJS350-22 ductile cast iron. SEM in situ surface analysis corresponding to the following σ [MPa]–ε% values: (a) 400–2.5%,(b) 430–5%, (c) 445–6%.

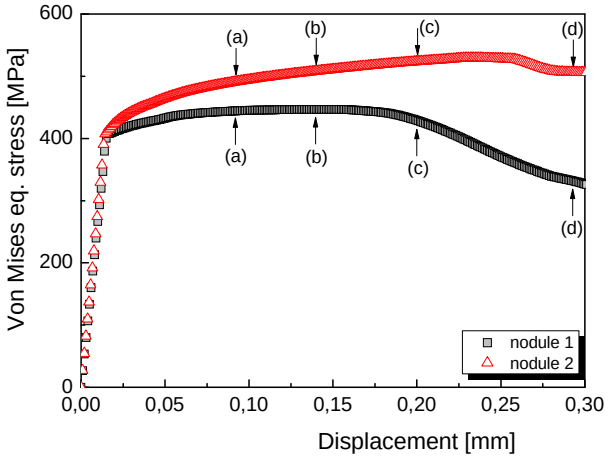

Figure 10. Evolution of Von Mises equivalent stress for two different points in the notched specimen.

It is evident that experimental results shown in Figs. 7-9 do no agree with references results obtained with analogous matrix microstructure and graphite nodules morphology (e.g. [4], Fig. 2).

In order to evaluate stress state on notched specimen, Von Mises stress analysis was performed considering ferritic DCI as a macroscopically homogeneous and isotropic material and using tensile test results obtained considering standard specimen as constitutive relationship. Fig. 10 shows FEM analysis results corresponding to two different nodules named “1” and “2”, with the corresponding deformation values considered for the “in situ” SEM damage analysis (named as point a, b, c and d, respectively).

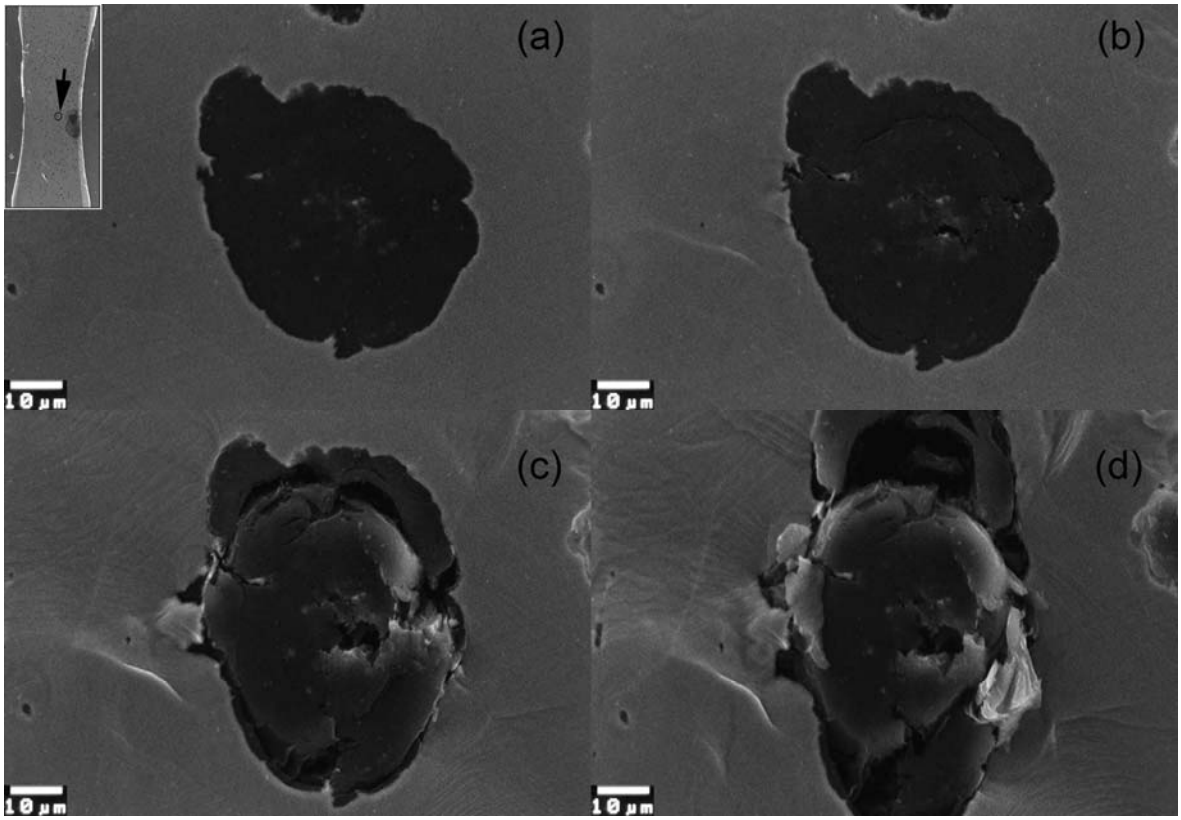

Figure 11. EN GJS350-22 ductile cast iron (nodule 1). SEM in situ surface analysis performed on notched specimen (arrow indicates investigated nodule).

Nodule 1 (in the center of the notched zone) is characterized by a crack initiation and “onion-like” damage mechanism corresponding to point b (Fig. 10 and 11 b), without evident slip lines in ferritic matrix. This initiation does not correspond to a decrease of Von Mises equivalent stress, probably due to the negligeable plastic deformation of ferritic matrix. From point c (Fig. 11 c and d), slip lines are more and more evident, and matrix plastic deformation is also characterized by evident cracks that nucleate

corresponding to the equator of the nodule. Fig. 11 d (almost specimen final rupture condition) is characterized by a really evident matrix deformation, with the "onion-like" damaging mechanism in the nodule that is completely developed.

Nodule 2 is characterized by an increase of Von Mises equivalent stress up to a displacement of about 250 μm (points a-c, Fig. 10). Points a – c are characterized by crack initiation and propagation in graphite nodules and by the emanation of slip lines. These slip lines are more and more evident with the increase of the deformation (Figs. 12 a – c). Point "d" in Fig 10 is characterized by a decrease of Von Mises equivalent stress: also in this case, cracks initiate in ferritic matrix (Fig. 12 d).

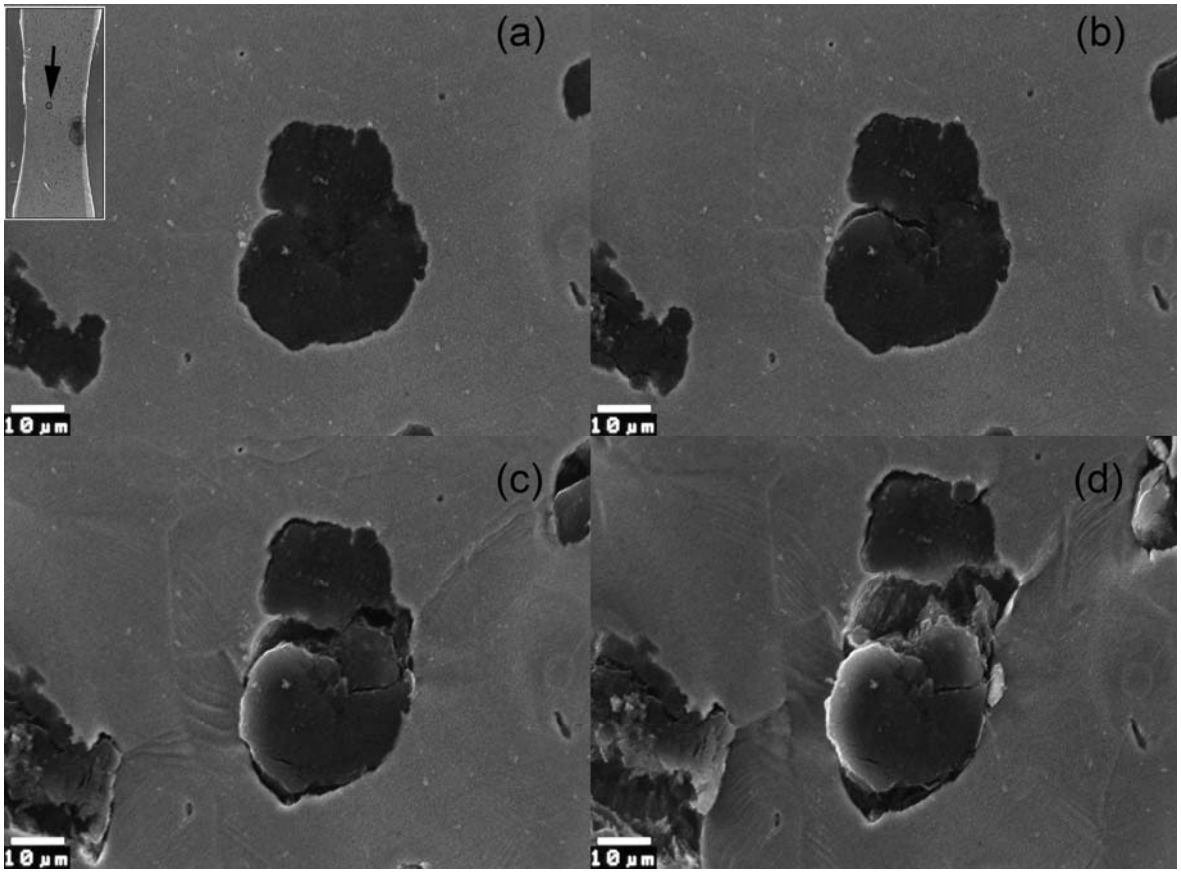

Figure 12. EN GJS350-22 ductile cast iron (nodule 2). SEM in situ surface analysis performed on notched specimen (arrow indicates investigated nodule).

Comparing Figs. 7 – 9 (unnotched specimen, uniaxial stress), with Figs. 11-12 (notched specimen), it is evident that ferritic matrix plastic deformation is more and more evident with the increase of triaxiality level. Furthermore, "pure" matrix-nodules debonding could not be considered as an evident damaging micromechanism.

Unfortunately, it wa not possible for the authors to modify the strain rate during tensile tests "in situ" and analyze the evolution of damage level: only a "traditional" SEM fracture surfaces observation was possible.

Very low strain rate value (1.3_x10^{-6} s^{-1}) corresponds to an evident presence of cleavage and secondary cracks (Fig.13a). Focusing graphite nodules (Fig 13b), they are characterized by a modified morphology (e.g., a hole in the right side of the nodule), probably due to crack initiation and propagation inside nodules and to the activation of of the "onion-like" damaging micromechanism. Considering that "in situ" tests were performed using an analogous low strain rate value (9.2 10^{-5} s^{-1}), fracture surface analysis results are consistent with the results obtained with tensile tests performed "in situ".

Fracture surfaces obtained with a higher strain rate value (6.7_x10^{-2} s^{-1}) do not show either cleavage or secondary cracks (Fig. 14a). Matrix microscopic ductile deformation is well developed both around graphite nodules (with an evident debonding and void growth) and with the presence of microdimples. Morphology degeneration of graphite nodules (Fig. 14b) seems to be less developed if compared with fracture surfaces obtained with lower strain rate values (Fig. 13b). This result seems to be consistent with the "pure" debonding micromechanism shown in references results (e.g. Fig. 2, [4]).

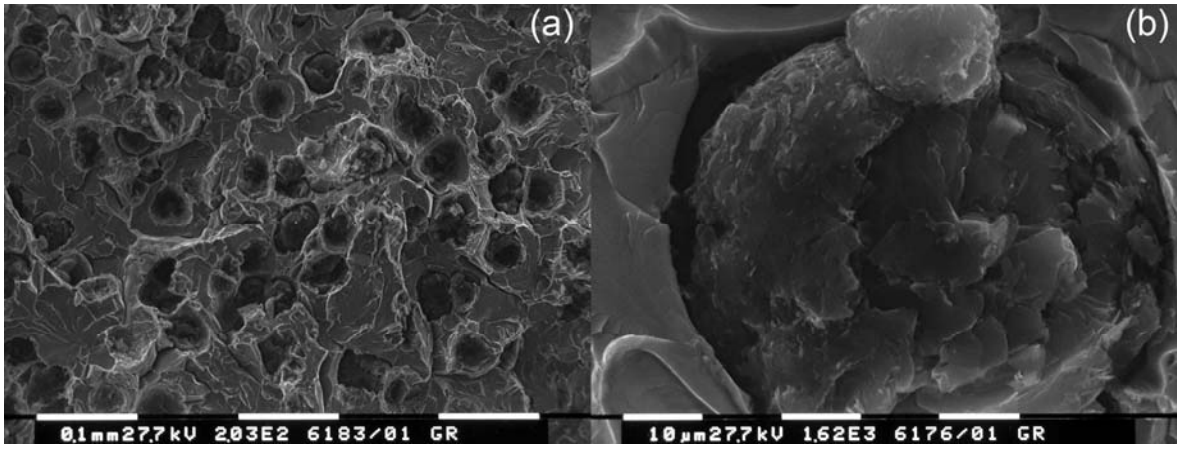

Figure 13. Fracture surface SEM analysis. Strain rate: 1.3_x10^{-6} s^{-1}.

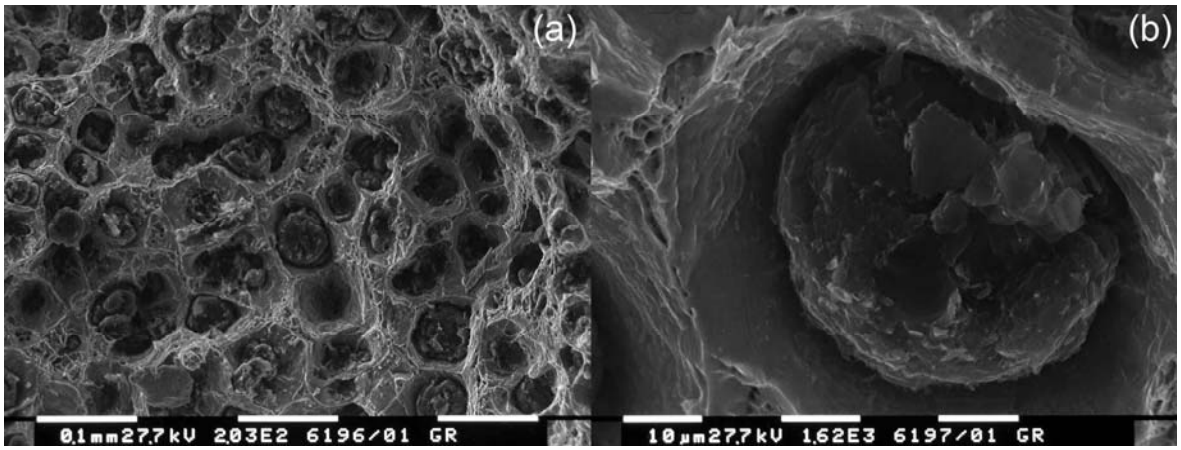

Figure 14. Fracture surface SEM analysis. Strain rate: 6.7_x10^{-2} s^{-1}.

CONCLUSIONS

Ferritic DCIs are characterized by good ductility, with tensile strength values that are equivalent to a low carbon steel. These ferrous alloys are characterized by a composite microstructure: ferritic matrix with graphite nodules embedded. References results focused on the analysis of DCI damaging micromechanisms consider as negligeable the role played by graphite nodules, identifying graphite nodules – ferritic matric ductile debonding, with the consequent void growth, as the main damaging micromechanisms.

In this work ferritic DCI damaging micromechanisms were investigated, considering uniaxial tensile tests, and analysing the influence of triaxiality and strain rate. Step by step tensile tests were performed on unnotched and notched specimens. Specimens surfaces were observed by means of a scanning electron microscope (SEM) during the test. Furthermore, tensile test were performed considering different deformation rates, performing a SEM observation of fracture surfaces.

On the basis of the experimental results, the following conclusions can be summarized:

- considering unnotched specimens, an “onion-like” mechanism is often observed, and the possibility to initiate and propagate a crack inside graphite nodule is not negligeable; “pure” ferritic matrix – graphite nodule debonding is not observed; evidences of ferritic matrix plastic deformation (slip lines) are obtained only after cracks initiation in graphite nodules.
- considering notched specimens, cracks initiation and propagation inside graphite nodules is more evident; the emanation of slip lines is more and more evident with the deformation increase, but a decrease of Von Mises equivalent stress is observed only corresponding to crack initiation in ferritic matrix. “Pure” graphite nodules –ferritic matrix deboning is not observed.
- strain rate seems to have a greater influence on the role played by graphite nodules on damaging micromechanisms. Lower strain rate values correspond to a more fragile fracture surface, with cleavage and secondary cracks in ferritic matrix and an evident modification of the morphology of graphite nodules, probably due to the activation of the “onion-like” mechanism and to crack initiation and propagation inside graphite nodules. Higher strain rates correspond to a more ductile fracture surface, with microdimples and an evident graphite nodules – ferritic matrix debonding: graphite nodules seems to be substantially unchanged.

REFERENCES

1. Ward R.G. , *An Introduction to the Physical Chemistry of Iron and Steel Making*, (1962) Arnold, London.
2. Labrecque, C. and Gagne, M. (1998) *Can. Metall. Quart*., **37**, 343–378.
3. http://www.msm.cam.ac.uk/phasetrans/2001/adi/cast.iron.html
4. Dong, M. J., Prioul, C. and François, D. (1997) *Metall. And Mater. Trans. A*, **28A**, 2245 – 2254.

5. Guillermer-Neel, C., Feaugas, X. and Clavel, M. (2000) *Metall. And Mater. Trans. A*, **31A**, 3063 – 3074.
6. J.H. Liu, Hao, X.Y., Li, G. L. and Liu, G. Sh. (2002) *Mater. Letters*, **56**, 748-755.
7. Voigt, R. C., Eldoky, L. M. and Chiou, H.S. (1986) *AFS Trans*., **94**, 645-656.
8. Eldoky, L. and Voigt, R.C. (1986) *AFS Trans*., **86-104**, 631-636.
9. Iacoviello, F., Di Cocco, V., Piacente, V. and Di Bartolomeo, O. (2008) *Mater. Science and Engng. A*, **478**, 181 – 186
10. Dai, P.Q., He, Z.R., Zheng, C.M. and Mao, Z.Y. (2001) *Mater. Science and Engng. A*, **319-321**, 531-534.